Author Manuscript

Author Manuscript

Author Manuscript

Author Manuscript

HHS Public Access

Author manuscript

Mol Biosyst. Author manuscript; available in PMC 2016 July 01.

Published in final edited form as:

Mol Biosyst. 2015 July ; 11(7): 1897–1906. doi:10.1039/c5mb00032g.

A metabolomic study of adipose tissue in mice with a disruption of the circadian system

C. Castro[a,*], **W. Briggs**[a,*], **G. K. Paschos**[b,*], **G. A. FitzGerald**[b], and **J. L. Griffin**[a,c]

[a]Department of Biochemistry and Cambridge Systems Biology Centre, University of Cambridge, 80 Tennis Court Road, Cambridge, CB2 1GA, UK

[b]Perelman School of Medicine, Institute for Translational Medicine and Therapeutics, University of Pennsylvania, 3400 Civic Center Boulevard, Philadelphia, PA 19104-5158, Pennsylvania, USA

[c]Human Nutrition Research, Medical Research Council, Elsie Widdowson Laboratory, 120 Fulbourn Road, Cambridge, CB1 9NL, UK

Abstract

Adipose tissue functions in terms of energy homeostasis as a rheostat for blood triglyceride, regulating its concentration, in response to external stimuli. In addition it acts as a barometer to inform the central nervous system of energy levels which can vary dramatically between meals and according to energy demand. Here a metabolomic approach, combining both Mass Spectrometry and Nuclear Magnetic Resonance spectroscopy, was used to analyse both white and brown adipose tissue in mice with adipocyte-specific deletion of *Arntl* (also known as *Bmal1*), a gene encoding a core molecular clock component. The results are consistent with a peripheral circadian clock playing a central role in metabolic regulation of both brown and white adipose tissue in rodents and show that *Arntl* induced global changes in both tissues which were distinct for the two types. In particular, anterior subcutaneous white adipose tissue (ASWAT) tissue was effected by a reduction in the degree of unsaturation of fatty acids, while brown adipose tissue (BAT) changes were associated with a reduction in chain length. In addition the aqueous fraction of metabolites in BAT were profoundly affected by Arntl disruption, consistent with the dynamic role of this tissue in maintaining body temperature across the day/night cycle and an upregulation in fatty acid oxidation and citric acid cycle activity to generate heat during the day when rats are inactive (increases in 3-hydroxybutyrate and glutamate), and increased synthesis and storage of lipids during the night when rats feed more (increased concentrations of glycerol, choline and glycerophosphocholine).

Introduction

Energy homeostasis is a multi-faceted cellular process, responsible for the integration of regulation and feedback loops that govern the dynamic and intricate interplay between

*These authors equally contributed to the paper.

†Footnotes should appear here. These might include comments relevant to but not central to the matter under discussion, limited experimental and spectral data, and crystallographic data.

Electronic Supplementary Information (ESI) available: from the journal's website. See DOI: 10.1039/b000000x/

Author Manuscript Author Manuscript Author Manuscript Author Manuscript

energy intake, storage and utilisation. Current evidence suggests a reciprocal relationship, of information exchange, between energy homeostasis and the circadian system. The circadian system, to which metabolic signals impose regulatory control, operates to coordinate energy mobilisation with diurnal changes in the environment [1] responding to feeding and activity levels. This regulatory system comprises an array of peripherally located clocks, in addition to the central clock of the suprachiasmatic nucleus (SCN) [2]. The SCN, located in the ventral hypothalamus, acts as the point of integration for these peripheral signals with light-dark information derived from the visual system [3]. In so doing, it effects their synchronisation.

A number of studies have suggested that disruption of the circadian system, also known as chronodisruption, may lead to obesity [4]. Consistent observations from different cohorts across the world, including northern and Mediterranean countries, showed that the important metabolic risk variables of obesity, raised triglyceride concentrations, and low HDL cholesterol concentrations were more common in shift workers than in day workers, even after adjustment for age and socioeconomic status [5, 6].

The molecular basis of the circadian cycle has been defined over the past twenty years [7]. Diurnal rhythmicity is achieved through a series of transcription-translation regulatory feedback loops [8] with positive and negative arms. A central component of the circadian cycle is *Arntl* (also known as *Bmal1*), a protein which heterodimerizes with Clock in the cytoplasm [9]. This complex then translocates to the nucleus where it binds with E-box elements to regulate gene transcription [10, 11].

Animal models demonstrate that, of these clock components, only universal disruption of *Arntl* [12] leads to a complete loss of both molecular and behavioural circadian rhythmicity [13], which in turn results in altered energy expenditure [14]. Additionally, mouse models have demonstrated that *Arntl* is integral to tissue specific peripheral clocks, and that these clocks can also play an essential role in the regulation of energy homeostasis. For example, liver specific deletion of *Arntl* results in aberrant buffering of circulating glucose [15].

Recently, we described a mouse model with an adipose tissue specific deletion of *Arntl* [16]. Detailed phenotyping, including lipidomic and transcriptional study of epididymal white adipose tissue and systemic metabolism in the form of blood plasma demonstrated the importance of the circadian rhythm as a modulator of the adipocyte-hypothalamic axis and its impact on body weight. Both short-term and long-term signals took part in the regulation of energy homeostasis: short-term changes had an immediate effect on food intake rhythmicity, which lead to an increase in body weight in the longer term.

To extend the results found in our previous study, we have examined metabolic changes in two other adipose tissue depots to examine how adipose tissue specific deletion of *Arntl* influences spatial disparity of function amongst fat stores. Specifically, we have used a combination of metabolomics and lipidomics to characterise and compare anterior subcutaneous white adipose tissue (ASWAT) and brown adipose tissue (BAT), demonstrating that *Arntl* has an important role in regulating metabolism in both tissues, and the responses are markedly different between white and brown adipose tissue.

Author Manuscript Author Manuscript Author Manuscript Author Manuscript

Results

Lipidomics of ASWAT demonstrates *Arntl* ablation profoundly effects triglyceride metabolism

We have previously demonstrated that Arntl ablation in adipose tissue alters the lipidomic profile of epididymal adipose tissue, particularly in terms of triglycerides containing polyunsaturated fats. However, other fat depots were not explored. Using multivariate statistics to examine the lipidomic data collected by LC-MS, PLS-DA demonstrated a clear separation between the control and Ad-*Arntl*$^{-/-}$ ASWAT mouse tissue metabolism regardless of time point (a two group comparison between genotype, regardless of time point, 1 latent variable from cross validation, R^2X=19.9%, R^2Y=68.3%, Q^2=57.7%; passed cross validation by random permutation) (Figure 1A), confirming the importance of *Arntl* in adipose tissue metabolism. The concentration of triglycerides TG(48:1) (composed of TG(16:1/16:0/16:0) and TG(18:1/16:0/14:0)), TG(48:2) (TG(16:1/16:1/16:0), TG(18:1/16:1/14:0) and TG(18:1/16:0/14:1)), TG(52:4) (TG(18:2/18:2/16:0) and TG(18:2/18:1/16:1)), TG(50:0) (TG(18:0/16:0/16:0)), TG(52:3) (TG(18:2/18:1/16:0)), TG(48:0) (TG(16:0/16:0/16:0)), TG(52:1) (TG(18:1/18:0/16:0)), TG(50:1) (TG(18:1/16:0/16:0) and TG(18:1/18:0/14:0)), TG(50:2) (TG(18:1/16:1/16:0) (TG(18:1/18:1/14:0)) were increased in Ad-*Arntl*$^{-/-}$ compared to control mice. Conversely, the concentration of triglycerides TG(54:3) (composed of TG(18:1/18:1/18:1) and TG(18:2/18:1/18:0) and TG(18:2/20:1/16:0))), TG(54:4) (TG(18:2/18:2/18:0) and TG(18:2/18:1/18:1), TG(54:5), TG(52:2) (TG(18:1/18:1/16:0), TG(50:3) (TG(18:2/16:1/16:0)) were decreased in Ad-*Arntl*$^{-/-}$ compared to control mice (Figure 1B). The observed changes demonstrated an increase in triglycerides containing short saturated fatty acids in the KO mice. In Figure 1C, a heat map with the ratio between lipids in Ad-*Arntl*$^{-/-}$ and control mice is shown, as a function of the numbers of carbon atoms and double bonds in the lipid. Blue spots indicate lipid species more concentrated in Ad-*Arntl*$^{-/-}$ mice, while red cells indicates lipids less concentrated in Ad-*Arntl*$^{-/-}$ mice, demonstrating the decrease of lipids with a high number of carbon atoms and double bonds in Ad-*Arntl*$^{-/-}$ mice. A systematic comparison between the two genotypes for a given time point was carried out and the results for the validated models are shown in Table S1 for each individual time point. The intact lipid profiles of Ad-*Arntl*$^{-/-}$ and control mice tissues were clearly separated at all individual time points demonstrating a difference associated with genotype at each time point. The next step in the analysis was a comparison between the different time points within the same genotype. PLS-DA models were built (Table S1), showing very small circadian changes in the intact lipid composition in adipose tissue from Ad-*Arntl*$^{-/-}$ mice when comparing different time points and no changes in the control mice. This suggests that in ASWAT, the fraction of triglycerides being synthesised or hydrolysed is relatively small compared to the total triglyceride content. This is possibly due to the function of the subcutaneous adipose playing a much smaller role in energy storage/release compared to the epididymal adipose tissue previously measured.

To investigate further the lipid composition, we performed a gas chromatography flame ionization detector (GC-FID) analysis to examine the total fatty acid content of the tissue. Clear discrimination was evident on a PLS-DA plot between the profiles from control and

Author Manuscript Author Manuscript Author Manuscript Author Manuscript

Ad-*Arntl*$^{-/-}$ mouse tissue ignoring time differences in this analysis (2 latent variables from cross validation, R^2X=37.4%, R^2Y=90.4%, Q^2=82.6%), confirming the importance of *Arntl* in the regulation of fatty acid metabolism (Figure 2A). The major metabolic changes that drive this separation were differences in the tissue composition of saturated and mono-unsaturated-fatty acids, with increased concentrations of saturated fatty acids (in particular C17:0, C16:0 and C18:0) in the Ad-*Arntl*$^{-/-}$ mice tissue and decreases in mono-unsaturated fatty acids (in particular C16:1, C14:1 and C17:1) (Figure 2B and Figure 2C). Furthermore, these changes were also apparent when comparing wild type and Ad-*Arntl*$^{-/-}$ at individual time points (Table S2). Unlike for the analysis of intact lipids, no model was successfully built comparing different time points in the same genotype for changes in total fatty acid analysis. This may be due to a possible buffering role of *Arntl* in ASWAT, or a relatively low turnover of triglycerides compared to total triglyceride content.

In summary, the analysis of ASWAT confirms the differences in lipid composition between controls and Ad-*Arntl*$^{-/-}$ mice tissues, shown previously in epididymal white adipose tissue (16). However, for this tissue alterations in the circadian cycle are more subtle and only detectable for the intact lipid data, unlike previously in epididymal tissue where more profound and dynamic differences were apparent.

Lipidomics demonstrates a profound role of *Arntl* in regulating metabolism in BAT

Multivariate modelling using PLS-DA of the intact lipid data from BAT tissue collected by LC-MS demonstrated a clear separation between the control and Ad-*Arntl*$^{-/-}$ mouse tissue when comparing the two groups and ignoring any time effects (2 latent variable from cross validation, R^2X=35.7%, R^2Y=74.1%, Q^2=48.7%) (Figure 3A), confirming the importance of the gene *Arntl* in regulating lipid metabolism in BAT as well as different depots of WAT.

Similarly to white adipose tissue, the relative concentrations of triglycerides were modified by a failure to express *Arntl*. TG(48:1) (composed of TG(16:1/16:0/16:0) and TG(18:1/16:0/14:0)), TG(52:3) (TG(18:2/18:1/16:0)), TG(48:0) (TG(16:0/16:0/16:0)), TG(50:1) (TG(18:1/16:0/16:0) and TG(18:1/18:0/14:0)), TG(50:2) (TG(18:1/16:1/16:0) and TG(18:1/18:1/14:0)), TG(52:2) (TG(18:1/18:1/16:0)) and TG(50:3) (TG(18:2/16:1/16:0)) were increased in Ad-*Arntl*$^{-/-}$ compared to control mice. Conversely, the concentrations of triglycerides TG(54:4) (TG(18:2/18:2/18:0) and

TG(18:2/18:1/18:1)) and TG(54:5), TG(54:2) (TG(18:1/18:0/18:1) were decreased in Ad-*Arntl*$^{-/-}$ compared to control mice (Figure 3B). Overall this indicated that a failure to express Arntl was associated with shorter chain fatty acids. These data indicate that in BAT the difference in lipid composition is associated more by alterations in the chain length, rather than the presence of double bonds as observed in ASWAT and epididymal WAT. Again, a heat map with the ratio between lipids in Ad-*Arntl*$^{-/-}$ and control mice in BAT as a function of the numbers of carbon atoms and double bonds in the lipid was formed (Figure 3C), demonstrating an decrease in longer chain fatty acids in the Ad-*Arntl*$^{-/-}$ mice regardless of degree of saturation. A systematic comparison between the two genotypes was carried (Table S3). As in the epididymal tissue but in contrast to ASWAT, Ad-*Arntl*$^{-/-}$ and control mice tissues were successfully separated when comparing individual time points for BAT. Contrary to what happens in ASWAT, changes in lipid composition were also detected

Author Manuscript Author Manuscript Author Manuscript Author Manuscript

in control mice comparing the different time points in the same genotype (as shown by the models built comparing T=6 with all the other possible time points), but this was only found for the first two time points for the Ad-*Arntl*$^{-/-}$ mice. This result suggests that lipid changes are driven by the day/night cycle in the tissue, influenced by *Arntl*.

To complement these results, GC-FID analysis of the lipid fraction was carried out, to characterize the total fatty acids present in it. Again a PLS-DA plot (Figure 4A) demonstrates a clear separation between the control and Ad-*Arntl*$^{-/-}$ mouse tissue regardless of time point (2 latent variables from cross validation, R^2X=52%, R^2Y=87%, Q^2=75.4%). Increased concentrations of C16:0, C14:0, C20:0, C14:1 and C12:0 and decreased concentrations of C18:0 and C18:1 were detected in Ad-*Arntl*$^{-/-}$ mice compared to controls (Figure 4B). These results are consistent with the previous findings from the analysis of the intact lipids, demonstrating that in BAT the length of the fatty acid chain is the important factor in differentiating the lipid composition of the two mice strains. Again, the relative proportions of the fatty acids were compared (Figure 4C). While the length of fatty acid discriminated between the mouse genotypes, no differences in saturated and monounsaturated fatty acids were detected between Ad-*Arntl*$^{-/-}$ and control mice in BAT, unlike described above in ASWAT.

The systematic comparison between all the possible pairs of tissues is summarised in Table S4. Again, Ad-*Arntl*$^{-/-}$ and control mice tissues were successfully discriminated when considering the individual time points. More subtle changes were present in lipid composition of the BAT across time, compared to ASWAT, as demonstrated by the number of models that it was possible to build between different time points belonging to the same genotype. However, no model was built considering day/night grouping either in the control or in the Ad-*Arntl*$^{-/-}$ mice, suggesting that fatty acids composition is regulated in a more complex way.

BAT plays a very different role in terms of systemic metabolism compared with WAT. While WAT contributes to energy homeostasis by acting largely as a store of fatty acids, BAT is a specialized tissue for energy expenditure, and in particular in adaptive thermogenesis, a physiological process during which energy is dissipated in response to environmental changes, including cold and increased consumption of dietary fat. The tissue contains high concentrations of mitochondria and as a result, a number of metabolites from the citric acid cycle and core metabolism. NMR spectroscopy of the aqueous fraction of BAT extracts was carried out to address in greater detail whether there are changes in these metabolic processes. Again, a PLS-DA plot revealed a clear separation (Figure 5A) between the control and Ad-*Arntl*$^{-/-}$ mouse tissue (3 latent variables from cross validation, R^2X=42.9%, R^2Y=87.9%, Q^2=61.8%). Thus, changes in the metabolic characteristics of Ad-*Arntl*$^{-/-}$ mice are not limited to the lipid fraction, but these metabolic changes extend to aqueous metabolites. Integral regions containing resonances belonging to *myo*-inositol (δ 3.26, 3.51, 3.61, 4.05,) glycerol (δ 3.54, 3.63) and choline (δ 4.05, 3.51) were increased in Ad-*Arntl*$^{-/-}$ mice compared to controls, while integral regions containing resonances belonging to taurine (δ 3.24, 3.40) were decreased in Ad-*Arntl*$^{-/-}$ mice compared to controls (Figure 5B).

Author Manuscript Author Manuscript Author Manuscript Author Manuscript

Again, a systematic comparison between the two genotypes at individual time points was carried out (Table S5). Ad-*Arntl*$^{-/-}$ and control mice tissues were successfully discriminated by these aqueous profiles. Furthermore, changes in the aqueous metabolites across time are present, as indicated by the number of models that it was possible to build between different time points belonging to the same genotype. The analysis of the models built considering the different time points demonstrated variation associated with the day/night cycle, as suggested by the successful separation between the night (T0 and T18) and the day (T6 and T12). The day night variation was associated in both cases with integral regions containing resonances belonging to glycerol (δ 3.54, 3.63, 3.76), taurine (δ 3.24) and glycerol-phosphocholine and phosphocholine (δ 3.20, 3.21), which were all increased during the night compared with the day, while integral regions containing resonances associated with glutamate (δ 2.05, 2.12) and 3-hydroxybutyrate (δ 2.29) were decreased during the night compared with the day.

The changes in triglyceride and phosphocholine metabolism suggest synthesis of lipids during the night while the animals are active and feeding, and an increase in oxidation of fatty acids and citric acid cycle activity as signified by increases in 3-hydroxybutyrate and glutamate during the day. While the majority of changes between day and night were consistent, considering the models built for Ad-*Arntl*$^{-/-}$ mice and controls, changes were detectable between the two genotypes. Two-way ANOVA shows significant different values between Ad-*Arntl*$^{-/-}$ mice and controls for taurine (p= 0.000126), glycerol (p=2.63E-05), lower in Ad-*Arntl*$^{-/-}$ mice, and myo-Inositol (p= 0.00187), higher in Ad-*Arntl*$^{-/-}$ mice, and for taurine (p=0.0053) and glycerol (p=0.00027) across time (Figure 5C, 5D and 5E).

In summary, the analysis of BAT tissue demonstrates that *Arntl* also has a profound impact on metabolism in this tissue as well as white adipose tissue, as proved by the different metabolic profiles of the two genotypes. Deletion of *Arntl* was associated with a general decrease in fatty acid chain length in triglycerides, in contrast to ASWAT tissue where there was a reduction in the degree of unsaturation. Differences across the time points in the day/night cycle are found in both strains considering both fatty acid and amino acid/central metabolism. The changes associated with the day/night circadian rhythm appear more pronounced in the Ad-*Arntl*$^{-/-}$ mice compared to controls, suggesting *Arntl* provides a homeostatic role, maintaining the composition of BAT despite changes in systemic metabolism associated with the day/night cycle.

Discussion

The two types of adipose tissues analysed here play very different roles in the body, with white adipose tissue contributing to energy homeostasis by acting as a store of energy and a rheostat for its release. Additionally, white adipose tissue acts as a barometer of energy storage, secreting leptin and other adipokines [17] and releasing fatty acids [18] into the circulation which signal adipose energy levels to the hypothalamus. The hypothalamus can then modulate energy intake and expenditure accordingly. We have previously found how *Arntl* influences this hypothalamus/white adipose tissue axis and influences weight gain [16]. Although both types of white adipose tissue are important storage sites for fat, they are functionally distinct, with ASWAT also playing important roles in insulation and tissue

Author Manuscript Author Manuscript Author Manuscript Author Manuscript

support. Moreover, subcutaneous, but not epididymal white adipose tissue may develop brown like adipocytes capable of thermogenesis in response to cold and adrenergic signalling [19]. BAT, on the other hand, is specialized for energy expenditure and in particular adaptive thermogenesis, a physiological process during which energy is dissipated in response to environmental changes such as cold exposure and high fat feeding by short circuiting oxidative phosphorylation using UCP1 [20, 21]. While central to temperature homeostasis in rodents and babies in humans, it has also been found to be significant in terms of energy expenditure in adult humans [22, 23]. Recent studies have demonstrated that it is involved in triglyceride clearance and glucose disposal [24], serves as a source of adipokines [25], and possesses distinct inflammatory function role comparable with WAT [26]. Furthermore, it may provide an important target for increasing energy expenditure and reducing obesity and improving insulin sensitivity.

The data presented in the current study are consistent with a peripheral circadian clock playing a central role in metabolic regulation of both brown and white adipose tissue in rodents. Analysis of ASWAT confirms our previous findings in the epididymal white adipose tissue that white adipose tissue from Ad-*Arntl*$^{-/-}$ mice differs in its lipid composition from controls as a result of the adipocyte specific disruption of the circadian clock [16]. The specific lipids changing are consistent with the observations reported in Paschos et al [16], where a decrease in the in the expression of genes responsible for the elongation (*Elovl6*) and desaturation (*Scd1*) of fatty acids were measured in Ad-*Arntl*$^{-/-}$ mice. The reduction in the expression of this desaturase gene was also described to be decreased in expression in the global and conditional *Bmal-1*$^{-/-}$ mice, showing that *Scd1* is partly under the control of *Arntl* at the whole organism level too [27]. Interestingly, it has been shown that the functional circadian clock in *Drosophila* appears to regulate the synthesis of pheromones by controlling the transcription of desaturase1, a gene required for the insertion of the double bonds in the phermones [28]. In addition the time trend for these lipid changes does not show dramatic differences across the day/night cycle, in agreement with a role of this tissue as “storage”, suggesting that changes occur across a long time span, more than in short cycles.

Analysis of BAT also demonstrated differences between the two strains, involving both lipid and aqueous metabolites, underlying the importance of *Arntl* gene in regulating central metabolism, energy expenditure and lipid mobilisation. In this case, the dominant factor in differentiating the lipid composition of the two genotypes is the increased proportion of shorter chain fatty acids in Ad-*Arntl*$^{-/-}$ mice compared to controls, in particular palmitate (16:0), suggesting a reduced oxidation rate of the fatty acids in the knockout mice. Furthermore, palmitate is the end product of de novo lipogenesis in liver and adipose tissue. The increased palmitate may reflect a mechanism to dispose of excess carbohydrate in the Ad-*Arntl*$^{-/-}$ mice, as a result of the global increase in obesity and alterations in white adipose tissue function as we previously reported [16]. Contrary to the results from ASWAT, in BAT differences in the day/night cycle were clearly detectable as would be expected given the dynamic metabolic role of BAT.

In addition to the lipid analyses performed by mass spectrometry, NMR spectroscopy demonstrated changes in the aqueous metabolites of BAT. NMR spectroscopy has previously

Author Manuscript Author Manuscript Author Manuscript Author Manuscript

been used to follow aqueous metabolite changes in urine associated with the diurnal cycle [29]. In the present study, the concentration of taurine is significantly decreased in the *Ad-Arntl*$^{-/-}$ mice. This metabolite serves as a conjugation substrate for bile acids and certain other compounds, increasing their polarity and aqueous solubility, is involved in the solubilisation of lipids in the cytosol and is positively correlated with mitochondrial function in the skeletal muscle and the heart [30, 31]. The decrease in taurine may reflect mitochondrial dysfunction which could reduce fatty acid oxidation and produce the increase in short chain fatty acids we have detected.

Experimental

Animal husbandry

A single *loxP* site and a Neo cassette flanked by an additional *loxP* site and two Frt sites were introduced into the introns upstream and downstream of coding exon 4 in mice bearing a conditional *Arntl*fx allele as previously described [16]. Mice were fed on a standard chow diet prior to the study. Mice were kept under an artificial light/dark, day/night, cycle: Lights were turned on at T0 and off at T12. Sampling at T0 and T18 therefore reflects metabolism during the night whilst T6 and T12 reflects metabolism during the day. Mice were euthanized under infrared light for tissue collection under circadian time. Adipose tissues (50-100 mg wet weight) were dissected under light and frozen immediately in liquid nitrogen. Typically tissue was dissected within 1 minute post mortem. All procedures were kept constant between controls and *Arntl*$^{-/-}$ mice. Studies were performed in accordance with the protocol approved by the University of Pennsylvania Institutional Animal Care and Use Committee. Mouse genotypes were assessed by PCR on genomic DNA from tail tips.

Extraction of metabolites

Tissue extraction was performed using a modified method to that described by Le Belle and co-workers [32]. For each tissue sample, 600 μl of methanol:chloroform (2:1 v/v) was added to 20 mg of frozen tissue. After being pulverised in a tissue lyser (Qiagen, UK) for 2 minutes at a frequency of 17 s^{-1}, the sample was sonicated for 15 minutes. Following this, 200 μl of chloroform and 200 μl of water was added, then centrifuged for 10 minutes at 13,000 rpm. The separated aqueous and lipid phases were collected. The procedure was repeated twice. The organic fraction was left to dry in the fume hood under nitrogen gas overnight and the aqueous fraction was dried in an evacuated centrifuge.

Analysis of the aqueous extract

NMR spectroscopy—The dried extracts were dissolved in 600 μl D_2O, containing 0.05 mM sodium-3-(tri-methylsilyl)-2,2,3,3-tetradeuteriopropionate (TSP) (Cambridge Isotope Laboratories, MA, USA) as an internal standard for both chemical shift and concentration. The samples were analysed using an AVANCE II+ NMR spectrometer operating at 500.13 MHz for the ^1H frequency (Bruker, Rheinstetten, Germany) using a 5 mm TXI probe. Spectra were collected using a solvent suppression pulse sequence based on a one-dimensional version of the nuclear Overhauser effect spectroscopy (NOESY) pulse sequence to saturate the residual ^1H water signal (relaxation delay = 2 s, t_1 increment = 3 us, mixing time = 150 ms, solvent presaturation applied during the relaxation time and the mixing

Author Manuscript Author Manuscript Author Manuscript Author Manuscript

time). One hundred and twenty-eight transients were collected into 16 K data points over a spectral width of 12 ppm at 27 °C.

Analysis of the lipid extract by GC-FID and LC-MS—The lipid fraction was reconstituted in 400 μl chloroform/methanol (1:1 v/v) prior to analysis.

Gas chromatography flame ionization detector (GC-FID) analysis of total fatty acids—50 μl of D-25 tridecanoic acid (200 μM in chloroform), 650 μl of chloroform/methanol (1:1 v/v) and 125 μl BF_3/methanol (Sigma-Aldrich) was added to 100 μl of the lipid extract. The samples were then incubated at 80 °C for 90 min. 500 μl H_2O and 1 ml hexane were added, the organic layer separated and dried under a stream of nitrogen as described previously [33]. The sample was reconstituted in 200 μl of hexane and analyzed on a Focus GC followed by the introduction of the eluent into a FID (Thermo Electron Corporation, Hemel Hempstead, UK). A TR-fatty acid methyl ester (FAME) stationary phase (GC) column (Thermo Electron; 30 m × 0.25 mm ID × 0.25 μm; 70% cyanopropyl polysilphenylene-siloxane) was used with a split ratio of 50. The injector temperature was 230°C and the helium carrier gas flow rate was 1.2 ml/min. The column temperature was 60°C for 2 min, increased by 15°C/min to 150°C, and then increased at a rate of 4°C/min to 230°C. Peaks were assigned using Food Industry FAME Mix (Restek 6098).

LC-MS analysis of intact lipids—50 μl of the original samples was added to a further 450 μl of methanol:chloroform (1:1 v/v). 10 μl was mixed with 1 ml of isopropyl alcohol (IPA):acetonitrile:water (2:1:1 v/v).

The samples were analyzed by LC-MS using a Waters quadrupole-time of flight (Q-ToF) G2 Xevo (Waters Ltd, Manchester, UK) interfaced with an Acquity Ultra Performance Liquid Chromatogram (UPLC). Five μl of the sample was injected onto a 1.7 μm bridged ethyl hybrid C8 column (2.1 × 100 mm; Waters Corporation, Manchester, UK) held at 55°C. The binary solvent system (flow rate 0.400 ml/min) consisted of solvent A which contained high performance liquid chromatography (HPLC) grade acetonitrile and water (60:40) with 10 mM ammonium formate) (solvents and chemicals from Sigma-Aldrich, Gillingham, Dorset) and solvent B HPLC grade acetonitrile:isopropanol (10:90) and 10 mM ammonium formate (solvents and chemicals from Sigma-Aldrich, Gillingham, Dorset)). The gradient started from 60% A/40% B, reached 99% B in 18 min, then returned back to the starting condition and remained there for the next 2 min. The data was collected over the mass range of m/z 100–1200 with a scan duration of 0.2 sec and an interscan delay of 0.014 s. The source temperature was set at 120°C and nitrogen was used as the desolvation gas (600 L/h) at 280°C. The voltages of the sampling cone and capillary were 30 V and 3 kV, respectively and collision energy 4.6 V. As lockmass, a solution of 2 ng/μl leucine enkephaline (m/z 556.2771) in 50:50 acetonitrile:water was infused into the instrument at 3 μl/min [34]. Lipids were identified to two different levels of specificity. Where identification was performed only using exact mass and chromatography these species are reported in terms of total number of carbons and double bonds on the species (e.g. TAG(48:3)). However, where fragmentation patterns allowed the fatty acids to be assigned these are reported specifying the individual fatty acids (e.g. TAG(18:0/ 18:1/ 18:2). Note these specifications do not assign a given fatty acid to a given position to the lipid backbone.

Author Manuscript Author Manuscript Author Manuscript Author Manuscript

Data processing—NMR spectra were processed using ACD one-dimensional NMR processor (version 12, ACD, Toronto, Canada). Free induction decays were Fourier transformed following multiplication by a line broadening of 1 Hz, and referenced to TSP at 0.0 ppm. Spectra were phased and baseline corrected manually. Each spectrum was integrated using 0.01 ppm integral regions between 2.0 and 4.5, and 5.5–9.5 ppm. The spectral region for each sample was normalized such that the total sum of integrals for each sample was 1. For the integration of selected metabolites, Chenomx, version 7.0 (Chenomx, Edmonton, Canada) was used, using TSP as internal standard.

GC–FID chromatograms were analysed using Xcalibur, version 2.0 (Thermo Scientific), integrating each peak individually. Peaks were normalized such that the sum of peaks for each sample was 100.

LC-MS chromatograms were analysed using Micromass Markerlynx Applications Manager Version 4.1 (Waters Corporation). Peaks were normalized such that the sum of peaks for each sample was equal.

Multivariate analysis of metabolite profiles—Each set of metabolic profiles obtained were analysed by multivariate analysis. Datasets were imported into SIMCA-P 12.0 (Umetrics, Umea°, Sweden) for processing using principal components analysis (PCA) and partial least squares discriminate analysis (PLS-DA; a regression extension of PCA used for supervised classification). Proton NMR spectroscopy and LC-MS data were Pareto scaled, in which each variable was centred and multiplied by $1/(S_k)^{1/2}$ where S_k is the standard deviation of the variable. GC–MS data were scaled to unit variance by dividing each variable by $1/(S_k)$.

In each case, the following strategy was applied for the data analysis:

1. PCA and PLS-DA models were built to investigate the possible differences between Ad-*Arntl*$^{-/-}$ and control mice;
2. PLS-DA models were built comparing the different time points belonging to the same genotype, to investigate possible changes due to the day/night cycle;
3. When relevant, time trends for specific metabolites were built.

Validation of PLS-DA models were determined by considering the Q^2 score with a Q^2>50% deemed a cut-off for a robust model. In addition we checked model validation by performing random permutation tests (where class membership is scrambled to produce Q^2 scores to compare with the true Q^2 score) and cross validation (CV)-analysis of variance (ANOVA) (ANOVA of the residuals of the cross validated Y scores). Students T-test, one-way ANOVA and two-ways ANOVA were also used, as appropriate, to assess the statistical significance of the metabolic differences.

Conclusions

In conclusion, we have used a combination of mass spectrometry and NMR spectroscopy to follow metabolic changes in white and brown adipose tissue in a mouse model where the clock gene Arntl was knocked out selectively in adipose tissue. Arntl induced global

Author Manuscript Author Manuscript Author Manuscript Author Manuscript

changes in both tissues which were distinct for the two tissue types. While ASWAT tissue was effected by a reduction in the degree of unsaturation of fatty acids, BAT changes were associated with a reduction in chain length. In addition the aqueous fraction of metabolites were profoundly affected by Arntl disruption, consistent with the dynamic role of this tissue in maintaining body temperature across the day/night cycle.

Supplementary Material

Refer to Web version on PubMed Central for supplementary material.

Acknowledgments

The authors wish to thank the NIH (The Personalized NSAID Therapeutics Consortium (PENTACON); all), the Medical Research Council, UK (MC_UP_A90_1006; JLG, WB & CC), the BBSRC (Bb/H013539/2; bb/I000933/I; JLG), and the British Heart Foundation for their support (JLG).

Notes and references

1. Green CB, Takahashi JS, Bass J. The meter of metabolism. Cell. 2008; 134(5):728–42. [PubMed: 18775307]
2. Schibler U, Sassone-Corsi P. A Web of Circadian Pacemakers. Cell. 2002; 111(7):919–922. [PubMed: 12507418]
3. Albrecht U, Eichele G. The mammalian circadian clock. Curr Opin Genet Dev. 2003; 13(3):271–7. [PubMed: 12787789]
4. Froy O. The relationship between nutrition and circadian rhythms in mammals. Front Neuroendocrinol. 2007; 28(2-3):61–71. [PubMed: 17451793]
5. Karlsson B, Knutsson A, Lindahl B. Is there an association between shift work and having a metabolic syndrome? Results from a population based study of 27,485 people. Occup Environ Med. 2001; 58(11):747–52. [PubMed: 11600731]
6. Di Lorenzo L, et al. Effect of shift work on body mass index: results of a study performed in 319 glucose-tolerant men working in a Southern Italian industry. Int J Obes Relat Metab Disord. 2003; 27(11):1353–8. [PubMed: 14574346]
7. Lowrey PL, Takahashi JS. Mammalian circadian biology: elucidating genome-wide levels of temporal organization. Annu Rev Genomics Hum Genet. 2004; 5:407–41. [PubMed: 15485355]
8. Ko CH, Takahashi JS. Molecular components of the mammalian circadian clock. Hum Mol Genet. 2006; 15 Spec No 2:R271–7. [PubMed: 16987893]
9. Fu L, Lee CC. The circadian clock: pacemaker and tumour suppressor. Nat Rev Cancer. 2003; 3(5): 350–61. [PubMed: 12724733]
10. Kondratov RV, et al. BMAL1-dependent circadian oscillation of nuclear CLOCK: posttranslational events induced by dimerization of transcriptional activators of the mammalian clock system. Genes Dev. 2003; 17(15):1921–32. [PubMed: 12897057]
11. Hogenesch JB, et al. The basic-helix-loop-helix-PAS orphan MOP3 forms transcriptionally active complexes with circadian and hypoxia factors. Proc Natl Acad Sci U S A. 1998; 95(10):5474–9. [PubMed: 9576906]
12. Yu EA, Weaver DR. Disrupting the circadian clock: gene-specific effects on aging, cancer, and other phenotypes. Aging (Albany NY). 2011; 3(5):479–93. [PubMed: 21566258]
13. Bunger MK, et al. Mop3 is an essential component of the master circadian pacemaker in mammals. Cell. 2000; 103(7):1009–17. [PubMed: 11163178]
14. Turek FW, et al. Obesity and metabolic syndrome in circadian Clock mutant mice. Science. 2005; 308(5724):1043–5. [PubMed: 15845877]
15. Lamia KA, Storch KF, Weitz CJ. Physiological significance of a peripheral tissue circadian clock. Proc Natl Acad Sci U S A. 2008; 105(39):15172–7. [PubMed: 18779586]

Author Manuscript Author Manuscript Author Manuscript Author Manuscript

16. Paschos GK, et al. Obesity in mice with adipocyte-specific deletion of clock component Arntl. Nat Med. 2012; 18(12):1768–77. [PubMed: 23142819]
17. Ahima RS, et al. Role of leptin in the neuroendocrine response to fasting. Nature. 1996; 382(6588): 250–2. [PubMed: 8717038]
18. Pocai A, et al. Restoration of hypothalamic lipid sensing normalizes energy and glucose homeostasis in overfed rats. J Clin Invest. 2006; 116(4):1081–91. [PubMed: 16528412]
19. Seale P, et al. Prdm16 determines the thermogenic program of subcutaneous white adipose tissue in mice. J Clin Invest. 2011; 121(1):96–105. [PubMed: 21123942]
20. Nicholls DG V, Bernson S, Heaton GM. The identification of the component in the inner membrane of brown adipose tissue mitochondria responsible for regulating energy dissipation. Experientia Suppl. 1978; 32:89–93. [PubMed: 348493]
21. Kozak LP, et al. The mitochondrial uncoupling protein gene. Correlation of exon structure to transmembrane domains. J Biol Chem. 1988; 263(25):12274–7. [PubMed: 3410843]
22. Virtanen KA, et al. Functional brown adipose tissue in healthy adults. N Engl J Med. 2009; 360(15):1518–25. [PubMed: 19357407]
23. Cypess AM, et al. Identification and importance of brown adipose tissue in adult humans. N Engl J Med. 2009; 360(15):1509–17. [PubMed: 19357406]
24. Bartelt A, et al. Brown adipose tissue activity controls triglyceride clearance. Nat Med. 2011; 17(2):200–5. [PubMed: 21258337]
25. Chartoumpekis DV, et al. Brown adipose tissue responds to cold and adrenergic stimulation by induction of FGF21. Mol Med. 2011; 17(7-8):736–40. [PubMed: 21373720]
26. Fitzgibbons TP, et al. Similarity of mouse perivascular and brown adipose tissues and their resistance to diet-induced inflammation. Am J Physiol Heart Circ Physiol. 2011; 301(4):H1425–37. [PubMed: 21765057]
27. Shimba S, et al. Deficient of a clock gene, brain and muscle Arnt-like protein-1 (BMAL1), induces dyslipidemia and ectopic fat formation. PLoS One. 2011; 6(9):e25231. [PubMed: 21966465]
28. Krupp JJ, et al. Social experience modifies pheromone expression and mating behavior in male Drosophila melanogaster. Curr Biol. 2008; 18(18):1373–83. [PubMed: 18789691]
29. Slupsky CM, et al. Investigations of the effects of gender, diurnal variation, and age in human urinary metabolomic profiles. Anal Chem. 2007; 79(18):6995–7004. [PubMed: 17702530]
30. Huxtable RJ. Expanding the circle 1975-1999: sulfur biochemistry and insights on the biological functions of taurine. Adv Exp Med Biol. 2000; 483:1–25. [PubMed: 11787586]
31. Bollard ME, et al. A study of metabolic compartmentation in the rat heart and cardiac mitochondria using high-resolution magic angle spinning 1H NMR spectroscopy. FEBS Lett. 2003; 553(1-2):73–8. [PubMed: 14550549]
32. Le Belle JE, et al. A comparison of cell and tissue extraction techniques using high-resolution 1H-NMR spectroscopy. NMR Biomed. 2002; 15(1):37–44. [PubMed: 11840551]
33. Morrison WR, Smith LM. PREPARATION OF FATTY ACID METHYL ESTERS AND DIMETHYLACETALS FROM LIPIDS WITH BORON FLUORIDE--METHANOL. J Lipid Res. 1964; 5:600–8. [PubMed: 14221106]
34. Roberts LD, et al. Metabolic phenotyping of a model of adipocyte differentiation. Physiol Genomics. 2009; 39(2):109–19. [PubMed: 19602617]

Author Manuscript
Author Manuscript
Author Manuscript
Author Manuscript

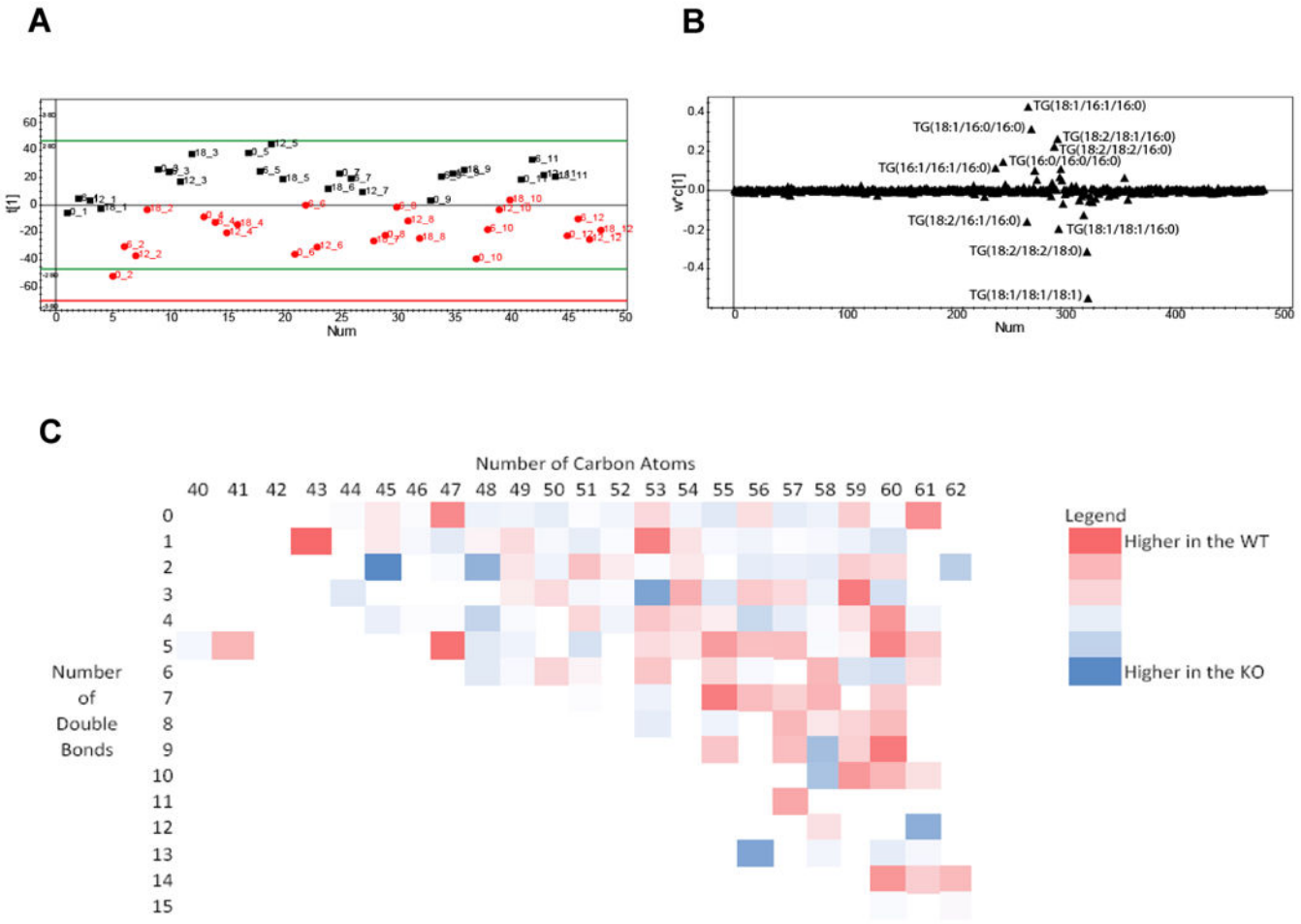

Figure 1.

A. Scores plot from a PLS-DA analysis showing the separation according to genotype between Ad-Arntl$^{-/-}$ and control mice in the fatty acid profiles obtained by LC-MS analysis of ASWAT. The black squares represent samples belonging to control animals, the red dots samples belonging to Ad-Arntl$^{-/-}$ mice. Numbers indicate the time point in hours and the animal number of that sample. **B**. Loading plot for the score plot in A, shows the lipids responsible for the discrimination between the groups. **C**. Heat map with the ratio between lipids in ASWAT in Ad-Arntl$^{-/-}$ and control mice, as a function of the numbers of carbon atoms and double bonds in the lipid. Blue circles indicate lipid species more concentrated in Ad-Arntl$^{-/-}$ mice, while red cells indicates lipids less concentrated in Ad-Arntl$^{-/-}$ mice.

Author Manuscript
Author Manuscript
Author Manuscript
Author Manuscript

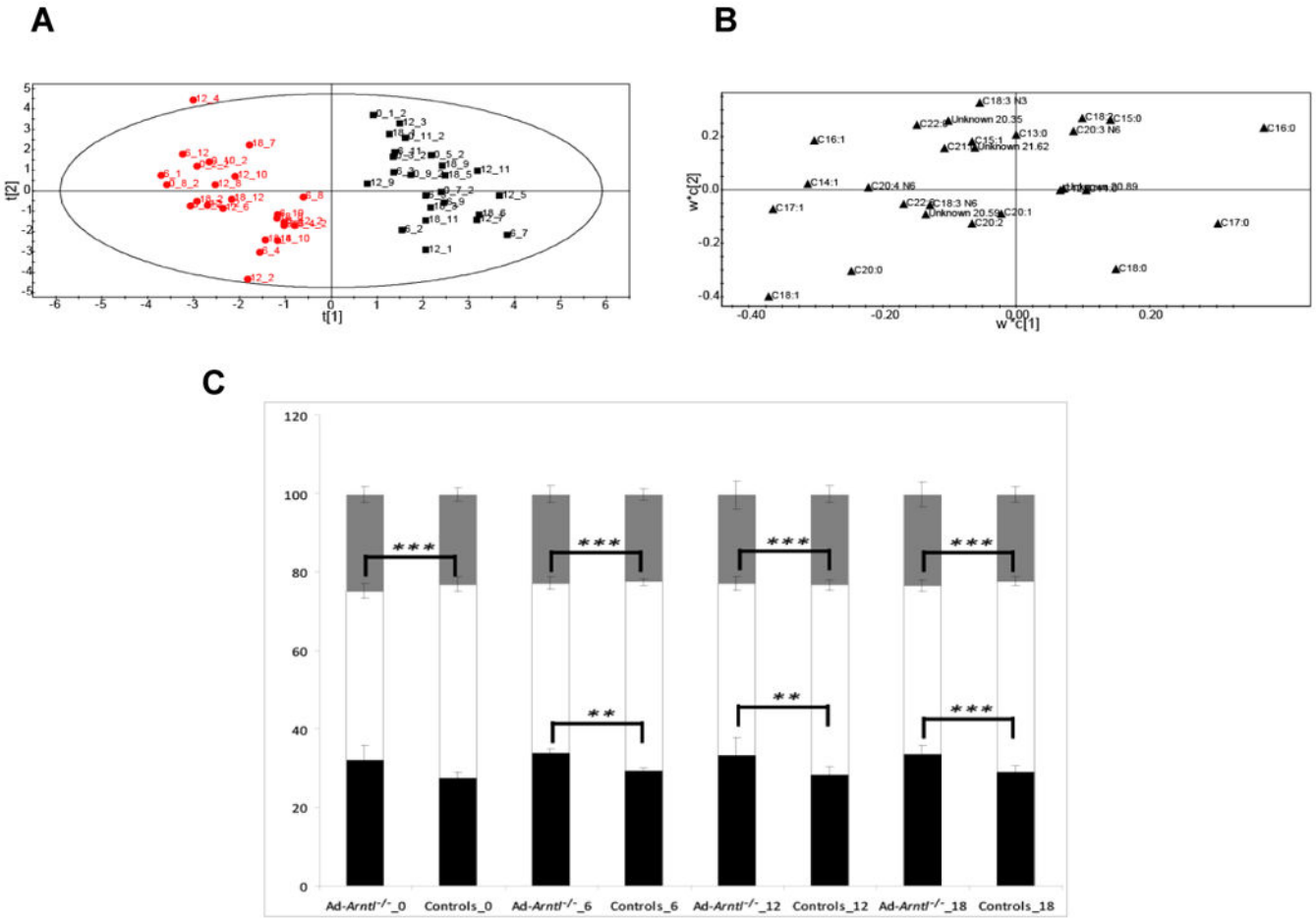

Figure 2.

A. Score plot showing the separation according to genotype between Ad-Arntl$^{-/-}$ and control mice in the fatty acid profiles obtained by GC-FID analysis of ASWAT. The black squares represent samples belonging to control animals, the red dots samples belonging to Ad-Arntl$^{-/-}$ mice. **B**. Loading plot for the score plot in A, shows the fatty acids responsible for the discrimination between the groups. **C**. Percentage of different types of fatty acids in ASWAT for Ad-Arntl$^{-/-}$ and control mice, at the different circadian time points. The per cent of each class was obtained combining the relative concentrations of all the fatty acids belonging to that class detected in the samples. Black bars represent saturated fatty acids, white bars monounsaturated fatty acids and grey bars polyunsaturated fatty acids. Stars indicate levels of significant differences in the percentage of types of fatty acids in Ad-Arntl$^{-/-}$ and control mice at each time as estimated by Students t-test: ** represent p-values between 0.01 and 0.001, *** represent p-values lower than 0.001.

Author Manuscript Author Manuscript Author Manuscript Author Manuscript

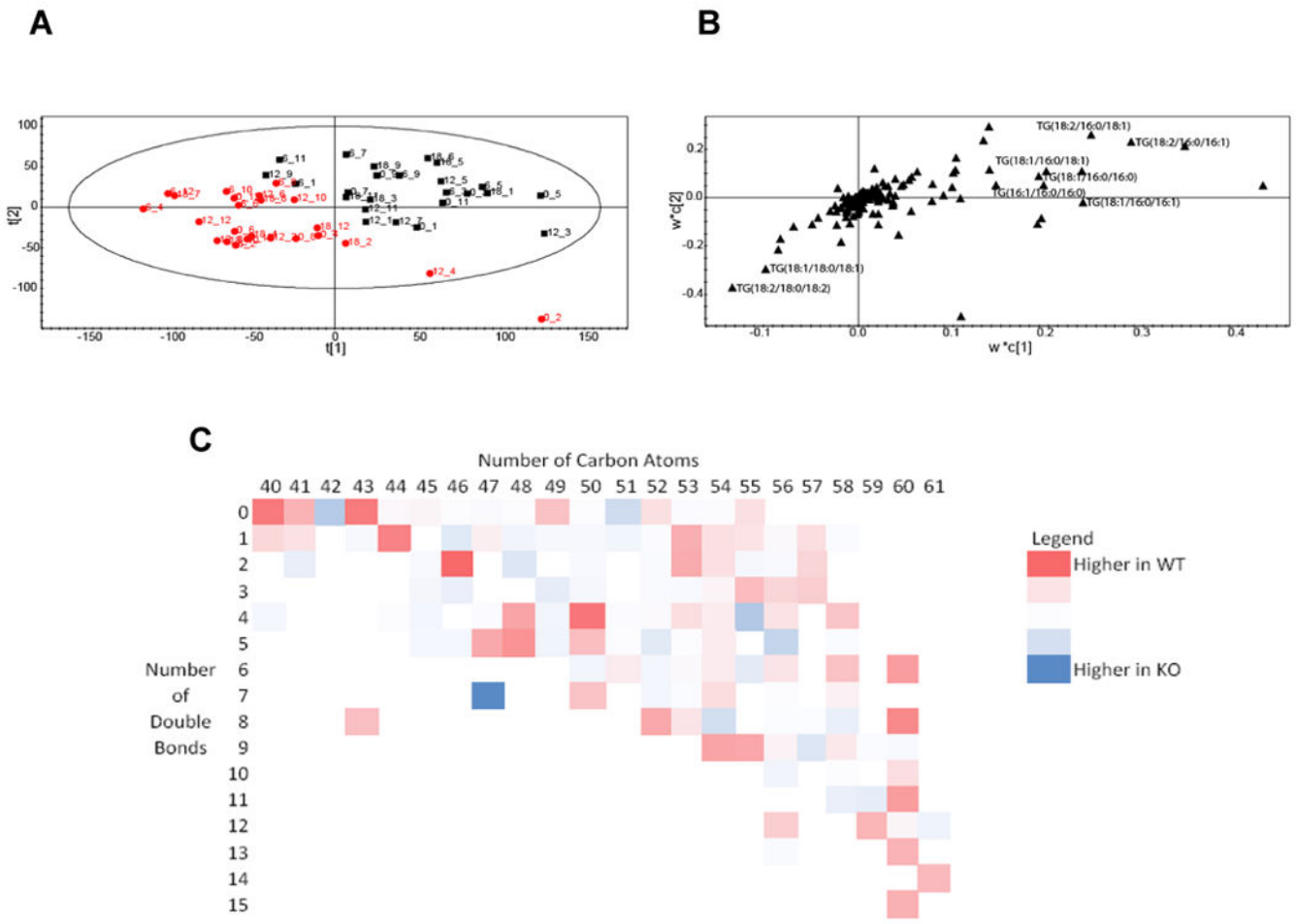

Figure 3.

A. Score plot showing the separation according to genotype between Ad-Arntl$^{-/-}$ and control mice in the fatty acid profiles obtained by LC-MS analysis of BAT. The black squares represent samples belonging to control animals, the red circles samples belonging to Ad-Arntl$^{-/-}$ mice. **B**. Loading plot for the score plot in A, shows the lipids responsible for the discrimination between the groups. **C**. Heat map with the ratio between lipids in BAT in Ad-Arntl$^{-/-}$ and control mice, as a function of the numbers of carbon atoms and number of double bonds in the lipid. Blue circles indicate lipid species more concentrated in Ad-Arntl$^{-/-}$ mice, while red cells indicates lipids less concentrated in Ad-Arntl$^{-/-}$ mice.

Author Manuscript
Author Manuscript
Author Manuscript
Author Manuscript

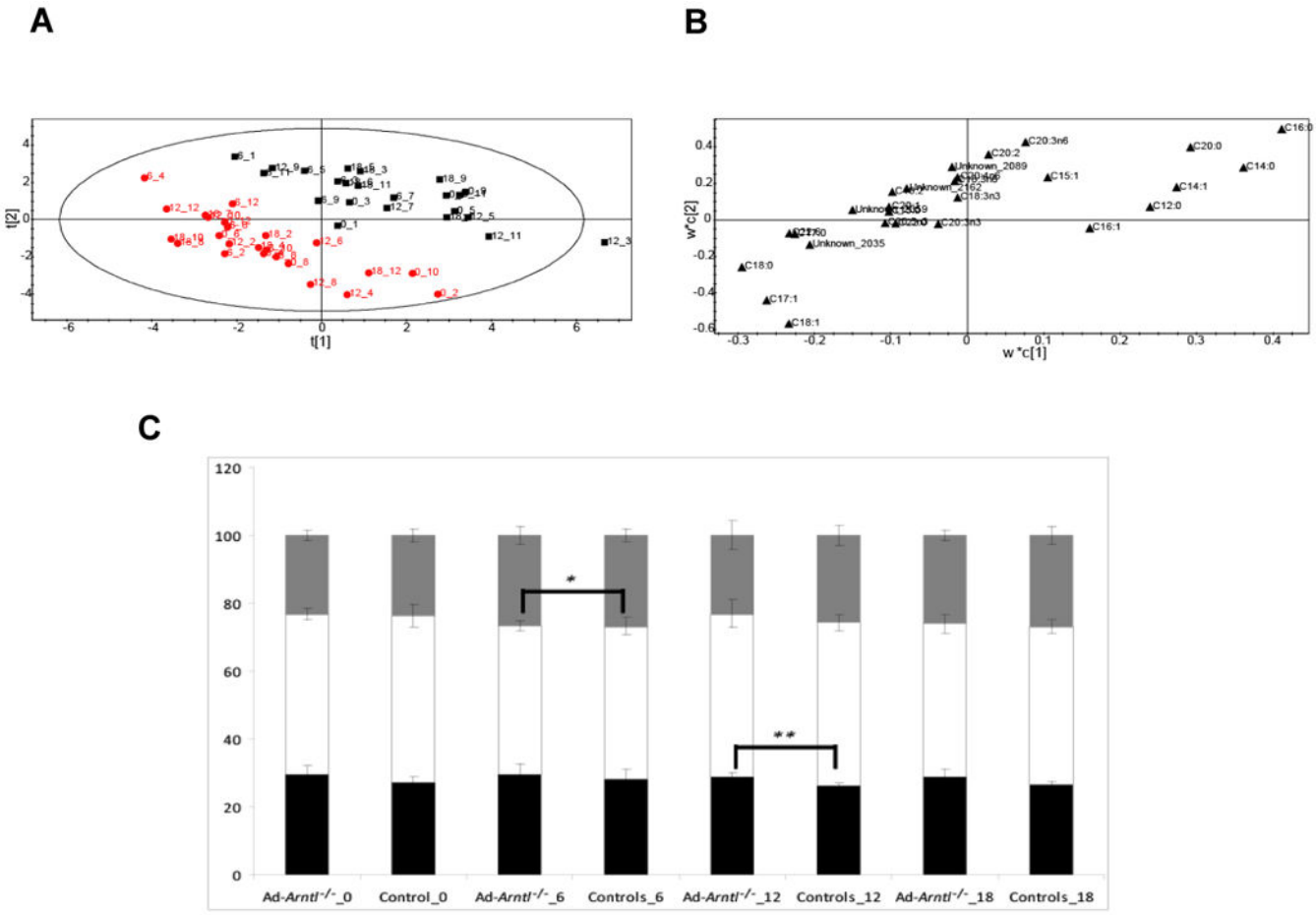

Figure 4.

A. Score plot showing the separation according to genotype between Ad-Arntl$^{-/-}$ and control mice in the fatty acid profiles obtained by GC-FID analysis of BAT. The black squares represent samples belonging to control animals, the red dots samples belonging to Ad-Arntl$^{-/-}$ mice. **B**. Loading plot for the score plot in A, shows the fatty acids responsible for the discrimination between the groups. **C**. Percentage of different types of fatty acids in BAT for Ad-Arntl$^{-/-}$ and control mice, at the different times. Black bars represent saturated fatty acids, white bars monounsaturated fatty acids and grey bars polyunsaturated fatty acids. Stars indicate levels of significant differences in the percentage of the different fatty acids in Ad-Arntl$^{-/-}$ and control mice at each time as estimated by t-test: ** represent p-values between 0.01 and 0.001, *** represent p-values lower than 0.001.

Author Manuscript Author Manuscript Author Manuscript Author Manuscript

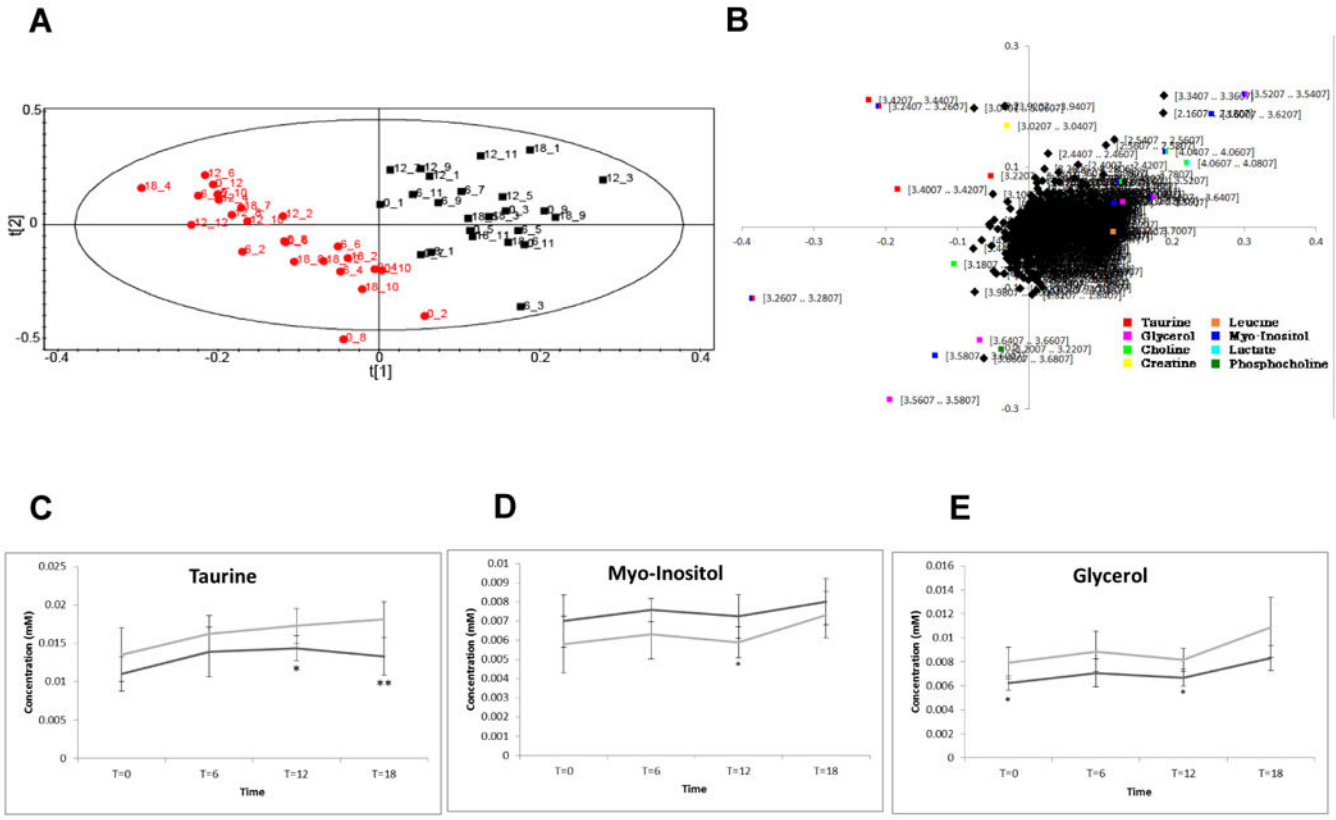

Figure 5.

A. Score plot showing the separation according to genotype between Ad-Arntl$^{-/-}$ and control mice in the aqueous profiles obtained by NMR analysis of BAT. The black squares represent samples belonging to control animals, the red dots samples belonging to Ad-*Arntl*$^{-/-}$ mice. **B**. Tables showing the regions of the spectra responsible for the discrimination between the groups in the score plot. **C**. Plot of the concentration of taurine with time. **D**. Plot of the concentration of myo-Inositol with time. **E**. Plot of the concentration of glycerol with time. In each case, the light grey line refers to control mice, the dark grey line to Ad-Arntl$^{-/-}$ mice. Integrals have been calculated from NMR spectra, normalising to internal standard and sample weight. The bars represent standard deviation. Stars indicate levels of significant differences as estimated by t-test: * represent p-values between 0.05 and 0.01, ** represent p-values between 0.01 and 0.001.